

## A Monomer Mott Insulator (BEDT-TTF)Cu[N(CN)<sub>2</sub>]<sub>2</sub> as a Potential Nodal Line System

Naoki Yoneyama<sup>1\*</sup>, Muhammad Khalish Nuryadin<sup>2</sup>, Takao Tsumuraya<sup>3</sup>, Satoshi Iguchi<sup>2</sup>,  
Takahiro Takei<sup>4</sup>, Nobuhiro Kumada<sup>4</sup>, Masanori Nagao<sup>4</sup>, Isao Tanaka<sup>4</sup>, and Takahiko Sasaki<sup>2</sup>

<sup>1</sup>Graduate Faculty of Interdisciplinary Research, University of Yamanashi, Kofu 400-8511, Japan

<sup>2</sup>Institute for Materials Research, Tohoku University, Sendai 980-8577, Japan

<sup>3</sup>Priority Organization for Innovation and Excellence, Kumamoto University, Kumamoto 860-8555, Japan

<sup>4</sup>Center for Crystal Science and Technology, University of Yamanashi, Kofu 400-0021, Japan

We report the band structure calculations and the experimental results of resistivity and magnetic susceptibility in a spin-1/2 (BEDT-TTF)<sup>•+</sup> monomer Mott insulator (BEDT-TTF)Cu[N(CN)<sub>2</sub>]<sub>2</sub>. The band calculations indicate a Dirac semimetal state with nodal lines at the Fermi level. The resistivity and the magnetic susceptibility as functions of temperature are well interpreted in terms of the monomer Mott insulating state instead of the expected semimetal state probably owing to strong electron correlation. In addition, we find that an Arrhenius-type steep reduction of the paramagnetic susceptibility appears below approximately 25 K, which indicates a spin-singlet ground state.

The electronic band structures with linear dispersion have recently been interested because of the mass-less Dirac nature of the fermion carriers. When the Fermi level is located near the center of the dispersion, the Dirac semimetal (DS) state can be achieved. The discovery of the quantum Hall effect in graphene<sup>1</sup> as a two-dimensional (2D) DS with the cone-type dispersion has begun to attract many studies. Especially, organic molecular based compounds are good platform to investigate the DS state in the bulk system. The first DS state in organics is recognized in a 2D layered system of  $\alpha$ -(BEDT-TTF)<sub>2</sub>I<sub>3</sub>,<sup>2</sup> and its relatives are recently developing,<sup>3,4</sup> where BEDT-TTF is bis(ethylenedithio)tetrathiafulvalene (abbreviated below as ET). The electronic band near the Fermi level in these systems is derived from the HOMO orbital of the ET molecule. On the other hand, in the single-component conductor [Pd(ddd)<sub>2</sub>], the DS state with nodal lines near the Fermi level comes from the HOMO and LUMO multi bands, which arises under pressure.<sup>5</sup> Moreover, [Pt(dmdt)<sub>2</sub>] realizes the node line DS state at ambient pressure.<sup>6</sup> Another interesting DS candidate is the three-dimensional (3D) diamond lattice system of (ET)Ag<sub>4</sub>(CN)<sub>5</sub> with a 1/2-filled band.<sup>7,8</sup>

We here focus on an ET salt with Cu(I) dicyanamide counter anion, (ET)Cu[N(CN)<sub>2</sub>]<sub>2</sub>,<sup>9</sup> which will be classified as a modified analogue of (ET)Ag<sub>4</sub>(CN)<sub>5</sub>. (ET)Cu[N(CN)<sub>2</sub>]<sub>2</sub> is a by-product of the organic dimer Mott insulator/superconductor  $\kappa$ -(ET)<sub>2</sub>Cu[N(CN)<sub>2</sub>]Cl ( $T_c = 12.8$  K under 0.3 kbar),<sup>9</sup> one of the most notable 2D-layered conducting systems composed of strongly dimerized ET molecules. In contrast to the dimer Mott system, (ET)Cu[N(CN)<sub>2</sub>]<sub>2</sub> could be considered as a spin-1/2 ET<sup>•+</sup> monomer Mott insulator. There is no 2D conducting sheet structure in (ET)Cu[N(CN)<sub>2</sub>]<sub>2</sub>, in which a peculiar 3D anisotropic diamond-like network of the ET molecules has been overlooked for decades.<sup>10</sup>

In the present paper, we investigate the band structure at room temperature (RT), revealing that the uniform zigzag chain with dihedral inter-chain (anisotropic diamond-like) interaction gives rise to a potential DS state with nodal lines. By means of X-ray crystal structure analysis, dc resistivity,

and static magnetic susceptibility measurements, the paramagnetic insulating properties are interpreted in terms of the monomer Mott insulating state.

Single crystals of (ET)Cu[N(CN)<sub>2</sub>]<sub>2</sub> were grown by conventional electrochemical method.<sup>9</sup> The black needle-like crystalline shape with a typical dimension of  $2 \times 0.05 \times 0.02$  mm<sup>3</sup> is easily distinguished by eyes from the thick platelet by-product of  $\kappa$ -(ET)<sub>2</sub>Cu[N(CN)<sub>2</sub>]Cl. We performed X-ray structural analysis at 296 and 100 K with different single crystals for temperature (Rigaku, XtaLAB mini and VariMax DW). For band calculations we adopt the crystallographic data taken from the literature,<sup>9</sup> where the coordinates of H and N atoms were optimized for the DFT calculation. In the tight-binding model, the intermolecular overlaps between the HOMO orbitals of ET were calculated on the basis of the extended Hückel method.<sup>11</sup> In the DFT band calculations, we employed projected augmented-wave pseudopotentials<sup>12,13</sup> with plane wave basis sets implemented in QUANTUM ESPRESSO.<sup>14</sup> The cutoff energies for plane waves and charge densities were set at 45 and 488 Ry, respectively. The exchange-correlation functional is the generalized gradient approximation by Perdew, Burke, and Ernzerhof.<sup>15</sup> The dimensions of the  $k$ -point mesh are  $12 \times 12 \times 12$ . The dc resistivity measurements at ambient pressure were carried out by means of conventional two- or four-terminal method, while quasi four-terminal method<sup>16</sup> with constant current of 0.1  $\mu$ A was adopted under pressure. A CuBe clamp-type hydrostatic pressure cell was used for the sample in the  $E \parallel c$  configuration up to 1.8 GPa with Daphne 7373 oil. The magnitude of pressure labeled below was estimated from the load gauge of the press machine at RT. A calibration of pressure performed distinctively using the superconducting transition of Pb showed the pressure loosen of approximately 0.3 GPa (at  $\sim 10$  K) until 2 GPa. Temperature was controlled with a PPMS system (Quantum Design, Dynacool). The temperature dependence of the static magnetic susceptibility was measured by a SQUID magnetometer (Quantum Design, MPMS-XL) using single crystals with a total of 1.1 mg. A batch of samples was placed inside a poly-acetal rod as the sample holder.

\*nyoneyama@yamanashi.ac.jp

The samples were inserted into the center of the rod without using any grease and the long axis of multiple crystals was positioned to be perpendicular to the applied field ( $H \perp c$ ). We obtained the magnetic susceptibility ( $\chi_{dc}$ ) after subtraction of the diamagnetic contribution using the Pascal's constant,  $\chi_{dia} = -3.6 \times 10^{-4}$  emu/mol, from the measured data.

First it will be useful to describe the crystal structure. The monoclinic ( $C2/c$ ) crystal structure reported previously<sup>9)</sup> is well reproduced at 296 K, and no significant variation is found at 100 K.<sup>17)</sup> One-half crystallographically independent ET molecule exists in the crystal structure of (ET)Cu[N(CN)<sub>2</sub>]<sub>2</sub>. The formal charge of ET is +1 because of the total valence of the anion (Cu(I)[N(CN)<sub>2</sub>]<sub>2</sub>)<sup>-1</sup>, and is in good accordance with the charge estimated from the intra-molecular bond length of ET at both 100 and 296 K. Figure 1(a) shows the crystal structure viewed from the ET molecular-long axis. The ET molecules form a 1D zigzag chain at regular intervals along the  $c$ -axis with the nearest intermolecular (diagonally side-by-side) S-S contact (bold red line,  $t$ ). There is a two-fold rotation axis perpendicular to the ET molecular plane, which guarantees the 1D chain to be uniform. In addition to the intra-chain coupling, the second-nearest interaction (blue wedge symbol,  $t'$ ) connects an ET with two others on the neighboring chains. Namely all the ET molecules are in distorted tetrahedral coordination geometry. The schematic view of the 3D network is shown in Fig. 1(b). Gray spheres (centroids of ET) construct the uniform 1D zigzag (red) chain along the  $c$ -axis, which is surrounded by four other chains via the (blue) couplings; this corresponds to the strongly anisotropic (almost 1D) diamond-like structure.

The polymeric anion is composed of a tetrahedral coordinate Cu(I) atom bridged by two bent dicyanamide anions (Fig. 1(c)) along the  $a + c$  direction. Because of the closed shell structure expected in the anion, it is almost likely that the anion does not contribute to the electronic state near the Fermi level and the properties such as conductivity and paramagnetism. Figure 1(d), the view from the  $a + c$  direction, indicates that the diamond-like packing of ET contains the columnar cavity occupied by the polymeric anions, resulting

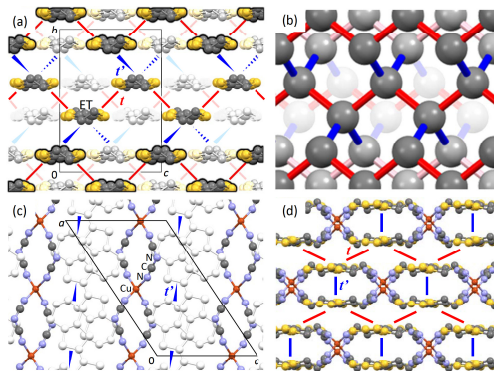


**Fig. 1.** (Color online) Crystal structure of (BEDT-TTF)Cu[N(CN)<sub>2</sub>]<sub>2</sub>. (a) View from the ET molecular long-axis shows the uniform 1D zigzag chains along the  $c$ -axis. The colored 1D chain through the middle of the unit cell is located on the  $bc$  plane. The bold and pale-colored ET motifs are in the front and rear sides, respectively. Anions are omitted for simplicity. (b) A diamond-like lattice corresponding to the ET stacking shown in (a). (c) View from the  $b$ -axis, showing the polymeric anion chain along the  $a + c$  direction in color. (d) View along the anion chain shown in (c).

in the unusual donor/anion mixed stacking structure.

We next explain the band structure calculated using the tight-binding model. The transfer integrals  $t$  and  $t'$  are estimated to be  $-0.192$  and  $+0.0229$  eV, respectively. Almost the same amounts of  $t (= -0.193$  eV) and  $t' (= +0.0227$  eV) using our X-ray data at 100 K are obtained, indicating that the band picture presented below is safely preserved at least down to 100 K. The conventional (monoclinic  $C$ ) unit cell is reduced to the primitive cell with the lattice vectors  $\mathbf{a}' = (\mathbf{a} - \mathbf{b})/2$ ,  $\mathbf{b}' = (\mathbf{a} + \mathbf{b})/2$ , and  $\mathbf{c}' = \mathbf{c}$ , as depicted in Fig. 2(a). The primitive cell constants are  $a' = b' = 10.886$  Å,  $\alpha' = \beta' = 115.45^\circ$ , and  $\gamma' = 79.63^\circ$  ( $V' = V/2 = 993.2$  Å<sup>3</sup> and  $Z' = Z/2 = 2$ ). The corresponding first Brillouin zone (BZ) is shown in Fig. 2(b) and we use the primitive cell for the band calculations.

On the basis of the standard tight-binding approximation, the matrix elements of the  $2 \times 2$  secular equation are  $H_{AA} = H_{BB} = 0$  and  $H_{AB} = H_{BA}^* = t + t'e^{-ik_c c'} + t'e^{ik_a a'} + t'e^{-ik_b b' - ik_c c'}$ . The energy dispersion is then obtained as

$$E_{\pm}(\mathbf{k}) = \pm 2 \sqrt{(t\alpha_k + t'\beta_k)^2 + 2t't\alpha_k\beta_k[\cos(a'k_a - b'k_b) - 1]}, \quad (1)$$

where  $\alpha_k = \cos(k_c c'/2)$  and  $\beta_k = \cos(k_a a'/2 + k_b b'/2 + k_c c'/2)$ . There are two band dispersions corresponding to the two equivalent ET molecules. Taking account of one electron-transfer from the HOMO of ET to the charge compensating anion, the Fermi level is located at the middle of the HOMO band, resulting in the 1/2-filled band. The empty upper ( $E_+$ ) and fully filled lower ( $E_-$ ) bands are symmetric with respect to the Fermi level and they contact at  $Z$  ( $k_a, k_b, k_c = (0, 0, \pi/c')$ ) as depicted in Fig. 2(c). This band degeneracy at  $Z$  comes from the zigzag uniform chain structure; by neglecting the small  $t' (\ll t)$ , one can reduce Eq. (1) to  $E_{\pm}(\mathbf{k}) \approx \pm 2|t \cos(k_c c'/2)|$ , leading to 1D “nodal” Fermi surfaces ( $00(\pm\pi/c')$ ) on  $Z$  with linear energy dispersion at around the 1st BZ. In the present system, the weak  $t'$  breaks the 1D Fermi degeneracy and contributes to leave nodal lines orthogonally crossing at  $Z$  as described below. The two nodal lines (i) and (ii) are obtained from Eq. (1) by using the condition  $E_{\pm}(\mathbf{k}) = 0$ :<sup>18)</sup> (i) is  $k_c c' = \pi$  and  $k_a a' + k_b b' = 0$ , and (ii)

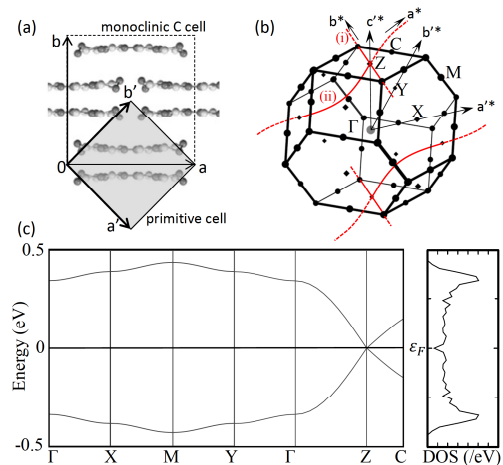


**Fig. 2.** (Color online) (a) Primitive unit cell ( $a'$ ,  $b'$ ) projected on the (001) plane of the conventional monoclinic  $C$  cell. (b) First Brillouin zone for the primitive cell with two nodal lines (i) and (ii). The solid and broken red curves express inside and outside of the BZ, respectively. (c) Band structure and the density of states (DOS) calculated within the tight-binding approximation.

$t \cos(k_c c'/2) + t' \cos(k_a a' + k_c c'/2) = 0$  and  $k_a a' - k_b b' = 0$ . The nodal lines are schematically depicted in Fig. 2(b). The node (i) is linear along the  $b^*$  ( $= -a^* + b^*$ )-axis on the 1st BZ, while the node (ii) is bending along the  $a^*$  ( $= a^* + b^*$ ) direction on the  $(1\bar{1}0)$  plane, that is the  $c^*a^*$ -plane in the monoclinic cell. As a result, strictly speaking, the present nodal feature originates not from the diamond-like structure ( $t'$ ) but from the zigzag uniform stacking along the  $c$ -axis ( $t$ ), corresponding to the existence of two equivalent sites in a primitive unit cell. Thus, if there is a slight modification in the uniform zigzag chain such as a perturbative dimerization of ET molecules, gap formation on all the nodal lines should easily occur.

Our tight-binding model based on the extended Hückel method generally reproduces the DFT band structure shown in Fig. 3. Although the bands derived from the anion orbitals overlap the lower HOMO band, they does not contribute to the formation of the Dirac-type dispersion.

We move on to the experimental results. Figure 4 shows the Arrhenius plot of the dc resistivity with the electric field parallel to three directions ( $a^*$ ,  $b$ , and  $c$ -axes). The most conductive direction is the  $c$ -axis (crystal long axis) with the resistivity of approximately 20  $\Omega\text{cm}$  at RT. The resistivities along the  $b$  and  $a^*$ -axes are 4 and 5 orders higher than that along the  $c$ -axis, respectively;  $\rho_c \ll \rho_b \leq \rho_{a^*}$ . The high anisotropy is consistent with the quasi-1D band dispersion. The behavior of the resistivity in whole the temperature range measured below  $\approx 200$  K can be explained as an insulator with an excitation energy  $E_a$  of approximately 0.13 eV (solid line in  $E \parallel c$ ), which is comparable with the previous study.<sup>9)</sup> A slight non-linearity of the Arrhenius plot is observed above 200 K, of which we confirmed high reproducibility by using several specimens. This deviation above 200 K will be related to the non-ohmic behavior (current-dependent  $\rho(T)$ ) observed recently.<sup>10)</sup>

The present salt has the 1/2-filled band, and thus a most reasonable interpretation of the insulating behavior is the scenario as a Mott insulator by the strong on-site Coulomb interaction  $U_{\text{eff}}$ . Since the localized site should be an ET molecule (monomer),  $U_{\text{eff}} = U_0 - V$ , where  $U_0$  is the on-site Coulomb interaction for an ideally isolated ET and  $V$  is the sum of the inter-site interactions.  $2E_a$  is equivalent to the Hubbard gap  $E_g = U_{\text{eff}} - W$ , where  $W$  is the band width. Applying  $E_a = 0.13$  eV obtained experimentally and  $W = 4|t - t'| = 0.86$  eV estimated from the tight-binding model, we obtain  $U_{\text{eff}} = 2E_a + W = 1.12$  eV. The magnitude of  $U_{\text{eff}}$  is almost

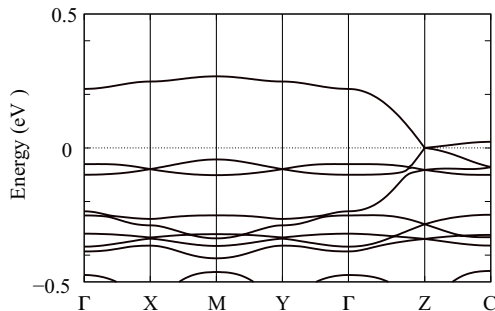


**Fig. 3.** Band structure of (BEDT-TTF)Cu[N(CN)<sub>2</sub>]<sub>2</sub> obtained by first-principles DFT calculations. The Fermi level is set to zero energy at the Dirac point Z (dotted line).

comparable to those of other monomer Mott insulators: 0.78 eV in (ET)Ag<sub>4</sub>(CN)<sub>5</sub><sup>19)</sup> and 0.82 eV in  $\zeta$ -(ET)PF<sub>6</sub>.<sup>20)</sup>

In the resistivity measured under pressure along the  $c$ -axis, the insulating behavior is still observed up to 1.8 GPa. As shown in the inset of Fig. 4,  $E_a$  monotonically decreases with increasing pressure. A rough extrapolation at the rate of  $dE_a/dP \approx -20$  meV/GPa (broken line in the inset) implies that pressure much higher than 5 GPa is needed to suppress the charge gap completely. The present salt seems to be robust against pressure, compared with (ET)Ag<sub>4</sub>(CN)<sub>5</sub>,  $dE_a/dP \approx -34$  meV/GPa.<sup>8)</sup> Unfortunately, in the latter salt, inevitable disorder in the anion (C/N site occupancy) disturbs the realization of the DS state under pressure. As a notable feature of the present salt, there is no such disorder in the anion Cu[N(CN)<sub>2</sub>]<sub>2</sub>. Thus if the crystal structure is safely preserved under pressure, the node line DS state can arise in a weak limit condition of electron correlation.

The localized carrier of (ET)Cu[N(CN)<sub>2</sub>]<sub>2</sub> has an  $S = 1/2$  spin degree of freedom as observed in ESR.<sup>9)</sup> The strong 1D network of ET suggests the low-dimensional feature in the temperature dependence of the paramagnetic susceptibility ( $\chi_{\text{para}}$ ). Figure 5 shows  $\chi_{\text{para}}(T)$  in 1 T (closed circles), which is obtained from  $\chi_{\text{dc}}(T)$  (open circles) after subtracting a Curie term of about 1.1% per ET molecule ( $\chi_{\text{imp}}(T)$ ). The amplitude of  $\chi_{\text{para}}$ , approximately  $2.3 \times 10^{-4}$  emu/mol at 300 K, monotonically decreases with decreasing temperature. Below  $\sim 25$  K, a steep exponential reduction of  $\chi_{\text{para}}$  is observed, indicating a spin-singlet ground state. The inset of Fig. 5 shows  $\chi_{\text{para}}(T)$  at low temperatures with an Arrhenius-type fitting of  $\exp(-\Delta/T)$  using  $\Delta = 90$  K.

Very recently a ferromagnetic transition at 13 K has been reported in wire-shape (ET)Cu[N(CN)<sub>2</sub>]<sub>2</sub>.<sup>10)</sup> However, reproducibility of the ferromagnetism has not been achieved as far as we examined it for several specimens with careful attention to avoiding contamination of by-products. The magnetic ground state is an open question at present, but our preliminary measurements of ESR at low temperatures show disappearance of the paramagnetic signal below approximately 25

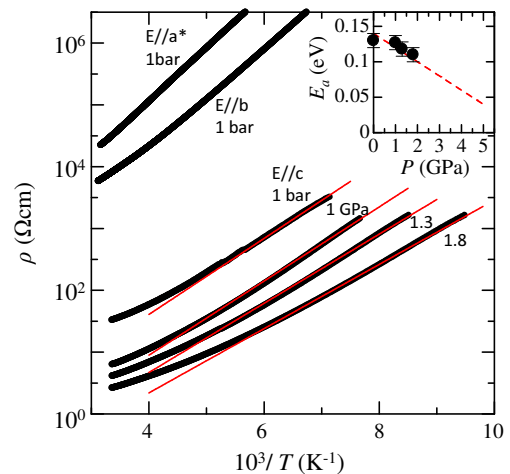


**Fig. 4.** (Color online) Arrhenius plot of the dc resistivity of (BEDT-TTF)Cu[N(CN)<sub>2</sub>]<sub>2</sub>. The anisotropic resistivities along the three directions are measured in ambient pressure; the resistivity under pressure is carried out in  $E \parallel c$ . The (red) solid lines are obtained by means of a linear fitting below 200 K, resulting in the pressure dependence of the activation energy (inset).

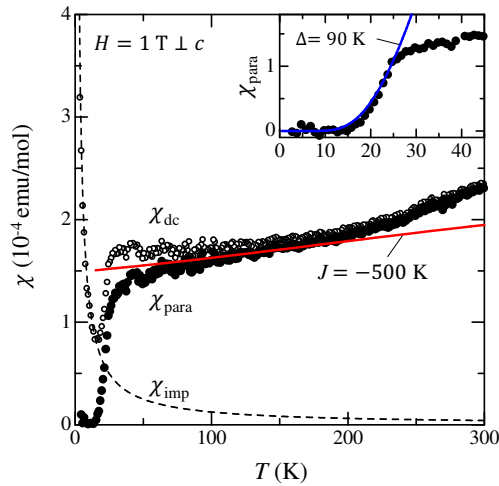


**Fig. 5.** (Color online) The temperature dependence of the magnetic susceptibility of (BEDT-TTF)Cu[N(CN)<sub>2</sub>]<sub>2</sub>.  $\chi_{\text{para}}$  (closed circles) is obtained after subtracting  $\chi_{\text{imp}}$  (broken curve) from  $\chi_{\text{dc}}$  (open circles). Fitting for  $\chi_{\text{para}}$  (red curve) is based on the 1D model.<sup>22)</sup> Inset is the enlargement of  $\chi_{\text{para}}(T)$  at low temperatures with an Arrhenius fitting (blue curve).

K, which is consistent with the present results of  $\chi_{\text{para}}(T)$  and the spin singlet state at low temperatures. The ESR study will be reported elsewhere.

We finally discuss the paramagnetic behavior. The gradual decrease of  $\chi_{\text{para}}$  from 300 K down to 25 K is explained as a typical short-range ordering which appears in the lower temperature regime of a broad peak in the susceptibility of the low-dimensional localized spin systems. By ignoring the inter-chain interaction originating from  $t'$ , the solid red curve in Fig. 5 is calculated on the basis of the  $S = 1/2$  Heisenberg antiferromagnetic spin model in the 1D lattice (Bonner-Fisher model,<sup>21,22)</sup> where the exchange interaction is defined as  $-2JS_i \cdot S_j$  with the intra-chain exchange interaction  $J = -500$  K and the Bohr magneton per ET of  $1.0 \mu_B$ . As another estimation of  $J$ , let the magnitude of  $2J$  to be equal to the energy gap between the singlet and triplet states in the 1D Hubbard model,  $(-U_{\text{eff}} + \sqrt{U_{\text{eff}}^2 + 16t^2})/2$ . With the parameters  $t = -0.19$  eV and  $U_{\text{eff}} = 1.12$  eV, we obtain  $|J| \approx 0.059$  eV (= 650 K), which is in good accordance with that from the fitting to  $\chi_{\text{para}}(T)$ . Although the fitting curve to  $\chi_{\text{para}}(T)$  is not quite satisfactory, this simple 1D model has suitable accuracy as a first-order approximation; the fitting may be improved by taking the inter-chain exchange interaction ( $t'$ ) into account.

In summary, we investigated the band structure, the resistivity, and the magnetic susceptibility in (ET)Cu[N(CN)<sub>2</sub>]<sub>2</sub>. The uniform zigzag chain interaction results in the potential DS state with the nodal lines, which could appear under pressure where the observed monomer Mott insulating state would be suppressed. The paramagnetic insulating electronic properties in the 1/2-filled band is well explained in terms of the Mott insulator. The sudden drop of  $\chi_{\text{para}}$  indicates a spin-singlet (non-magnetic) ground state below 25 K.

**Acknowledgment** The DFT calculations were conducted primarily at MASAMUNE at the Institute for Materials Research, Tohoku University, Japan. This work was performed under the GIMRT Program of the Institute for Materials Research, Tohoku University (Proposal No. 202012-RDKGE-0034), and partly supported by JSPS KAKENHI Grant No. 16K05747,

19K21860, 19H01833, 21H05471, 22H01149, and 22H04459.

- 1) K. S. Novoselov, A. K. Geim, S. V. Morozov, D. Jiang, M. I. Katsnelson, I. V. Grigorieva, S. V. Dubonos, and A. A. Firsov, *Nature* **438**, 197 (2005).
- 2) S. Katayama, A. Kobayashi, and Y. Suzumura, *J. Phys. Soc. Jpn.* **75**, 054705 (2006).
- 3) T. Naito, R. Doi, and Y. Suzumura, *J. Phys. Soc. Jpn.* **89**, 023701 (2020).
- 4) S. Kitou, T. Tsumuraya, H. Sawahata, F. Ishii, K. Hiraki, T. Nakamura, N. Katayama, and H. Sawa, *Phys. Rev. B* **103**, 035135 (2021).
- 5) R. Kato, H. Cui, T. Tsumuraya, T. Miyazaki, and Y. Suzumura, *J. Am. Chem. Soc.* **139**, 1770 (2017).
- 6) B. Zhou, S. Ishibashi, T. Ishii, T. Sekine, R. Takehara, K. Miyagawa, K. Kanoda, E. Nishibori, and A. Kobayashi, *Chem. Commun.* **55**, 3327 (2019).
- 7) Y. Shimizu, A. Otsuka, M. Maesato, M. Tsuchiizu, A. Nakao, H. Yamochi, T. Hiramoto, Y. Yoshida, and G. Saito, *Phys. Rev. B* **99**, 174417 (2019).
- 8) A. Kiswandhi, M. Maesato, S. Tomeno, Y. Yoshida, Y. Shimizu, P. Shahi, J. Gouchi, Y. Uwatoko, G. Saito, and H. Kitagawa, *Phys. Rev. B* **101**, 245124 (2020).
- 9) H. H. Wang, U. Geiser, J. M. Williams, K. D. Carlson, A. M. Kini, J. M. Mason, J. T. Perry, H. A. Charlier, A. V. S. Crouch, J. E. Heindl, M. W. Lathrop, B. J. Love, D. M. Watkins, and G. A. Yaconi, *Chem. Mater.* **4**, 247 (1992).
- 10) Y. Huang, T. Mitchell, D. C. Yost, Y. Hu, J. B. Benedict, J. C. Grossman, and S. Ren, *Nano Lett.* **21**, 9746 (2021).
- 11) T. Mori, A. Kobayashi, Y. Sasaki, H. Kobayashi, G. Saito, and H. Inokuchi, *Bull. Chem. Soc. Jpn.* **57**, 627 (1984).
- 12) P. E. Blöchl, *Phys. Rev. B* **50**, 17953 (1994).
- 13) A. Dal Corso, *Comp. Mater. Sci.* **95**, 337 (2014).
- 14) P. Giannozzi, O. Andreussi, T. Brumme, O. Bunau, M. B. Nardelli, M. Calandra, R. Car, C. Cavazzoni, D. Ceresoli, M. Cococcioni, N. Colonna, I. Carnimeo, A. D. Corso, S. de Gironcoli, P. Delugas, R. A. DiStasio, A. Ferretti, A. Floris, G. Fratesi, G. Fugallo, R. Gebauer, U. Gerstmann, F. Giustino, T. Gorni, J. Jia, M. Kawamura, H.-Y. Ko, A. Kokalj, E. Küçükbenli, M. Lazzeri, M. Marsili, N. Marzari, F. Mauri, N. L. Nguyen, H.-V. Nguyen, A. O. de-la Roza, L. Paulatto, S. Poncè, D. Rocca, R. Sabatini, B. Santra, M. Schlipf, A. P. Seitsonen, A. Smogunov, I. Timrov, T. Thonhauser, P. Umari, N. Vast, X. Wu, and S. Baroni: *J. Phys. Cond. Matter* **29**, 465901 (2017).
- 15) J. P. Perdew, K. Burke, and M. Ernzerhof, *Phys. Rev. Lett.* **77**, 3865 (1996).
- 16) A voltage terminal was also used as a current probe because the corresponding current lead was disconnected during pressure application.
- 17) The crystallographic data at 296 K are: formula C<sub>14</sub>H<sub>8</sub>S<sub>8</sub>CuN<sub>6</sub>, space group C2/c, Z = 4, a = 16.756(3) Å, b = 13.975(3) Å, c = 10.340(2) Å, β = 124.145(10)°, V = 2003.9(7) Å<sup>3</sup>, d<sub>calc</sub> = 1.923 g cm<sup>-3</sup>. R<sub>1</sub>(for I > 2σ(I), 1882 reflections) = 0.041, wR<sub>2</sub>(for all, 2306 reflections) = 0.1127, and Goodness of fit (GOF) = 1.099. The data at 100 K are: a = 16.781(3) Å, b = 13.816(3) Å, c = 10.3114(16) Å, β = 123.816(5)°, V = 1986.3(6) Å<sup>3</sup>, d<sub>calc</sub> = 1.940 g cm<sup>-3</sup>. R<sub>1</sub>(for I > 2σ(I), 2094 reflections) = 0.0374, wR<sub>2</sub>(for all, 2196 reflections) = 0.1184, and GOF = 1.332.
- 18) In the 1st BZ, always  $\alpha_k \geq 0$ . Thus, if  $\beta_k \geq 0$ , the condition  $E_{\pm}(k) = 0$  is fulfilled by the following two cases: (i)  $\alpha_k = \beta_k = 0$  or (ii)  $t\alpha_k + t'\beta_k = 0$  and  $\cos(a'k_x - b'k_y) - 1 = 0$ . We then obtain the two nodal lines as in the text. The node (i) linearly connects Z with e.g.,  $(a^*/2, -b^*/2, c^*/2)$ , while node (ii) is bending through e.g.,  $(-a^*/2, -b^*/2, c^*/2)$ . In case of  $\beta_k < 0$ , it is numerically confirmed that there is no solution for  $E_{\pm}(k) = 0$ .
- 19) A. Otsuka, Y. Shimizu, G. Saito, M. Maesato, A. Kiswandhi, T. Hiramoto, Y. Yoshida, H. Yamochi, M. Tsuchiizu, Y. Nakamura, H. Kishida, and H. Ito, *Bull. Chem. Soc. Jpn.* **93**, 260 (2020).
- 20) H.-L. Liu, L.-K. Chou, K. A. Abboud, B. H. Ward, G. E. Fanucci, G. E. Granroth, E. Canadell, M. W. Meisel, D. R. Talham, and D. B. Tanner, *Chem. Mater.* **9**, 1865 (1997).
- 21) J. C. Bonner and M. E. Fisher, *Phys. Rev.* **135**, A640 (1964).
- 22) W. E. Estes, D. P. Gavel, W. E. Hatfield, and D. J. Hodgson, *Inorg. Chem.* **17**, 1415 (1978).